through silica gel layer, carefully concentrated, and distilled in vacuo.

[5]-Triangulanes (4a,c and 4b). From 1.32 g (10 mmol) of a methylene-[4]-triangulane mixture **7**, 1.33 g (91%) of a mixture of **4a,c** and **4b** (3.7:1) was obtained: bp 70 °C (2 mm); n^{25}_D 1.4925; d^{20}_4 0.916. **4a,c**: ^{1}H NMR δ 0.62-0.86 (m, 8 H), 1.30 (s, 2 H), 1.45-1.60 (AB system δ_A = 1.47, δ_B = 1.57, J = 3.9 Hz); ^{13}C NMR, δ 4.30, 4.74, 10.95, 11.23 (CH_2), 13.81, 18.71 (C). **4b**: ^{1}H NMR δ 0.54-0.77 (m, 8 H), 1.12 (d, J = 4.3 Hz, 1 H), 1.13 (d, J = 3.7 Hz, 2 H), 1.21 (d, J = 3.7 Hz, 2 H), 1.24 (d, J = 4.3 Hz, 1 H); ^{13}C NMR δ 5.06, 7.13, 11.39, 12.90 (CH_2), 14.12, 19.50 (C). Calcd. for $C_{11}H_{14}$: C, 90.41; H, 9.59. Found: C, 89.99; H, 9.99.

[6]-Triangulanes (8a,f and 8b,e). From 0.79 g (5 mmol) of a methylene-[5]-triangulane mixture **6**, 0.8 g (93%) of a mixture of **8** (3:2) was obtained bp 85 °C (2 mm); n^{21}_D 1.5079. Compounds **8a,f** and **8b,e** were separated by GLC. **8a,f**: ^{1}H NMR δ 0.68-0.9 (m, 8 H), 0.95 (d, J = 3.9 Hz, 2 H), 1.16 (d, J = 3.8 Hz, 2H), 1.17 (d, J = 3.9 Hz, 2H), 1.19 (d, J = 3.8 Hz, 2 H); ^{13}C-^{1}H NMR δ 4.43 (t, J = 161.6 Hz), 4.85 (t, J = 161.4 Hz), 5.61 (s), 10.13 (t, J = 160.1 Hz), 11.24 (t, J = 160.2 Hz), 13.67 (s), 18.13 (s), 18.83 (s). **8b,e**: ^{1}H NMR δ 0.63-0.94 (m, 8 H), 0.98 (d, J = 3.7 Hz, 1 H), 1.01 (d, J = 3.7 Hz, 1 H), 1.07 (d, J = 3.9 Hz, 1 H), 1.12 (d, J = 3.7 Hz, 1 H), 1.16 (d, J = 2.3 Hz, 1 H), 1.18 (d, J = 2.3 Hz, 1 H), 1.24 (d, J = 3.7 Hz, 1 H), 1.29 (d, J = 3.7 Hz, 1 H); ^{13}C NMR δ 4.44, 4.85, 5.20, 7.21, 10.21, 11.93, 12.89, 13.03 (CH_2), 12.21, 13.91, 14.29, 19.96, 20.55 (C).

Fluorinated Macrocyclic Ethers as Fluoride Ion Hosts. Novel Structures and Dynamic Properties[1]

William B. Farnham,* D. Christopher Roe, David A. Dixon,* Joseph C. Calabrese, and Richard L. Harlow

Contribution No. 5360 from the Central Research & Development Department, E. I. du Pont de Nemours & Co., Inc., P.O. Box 80328, Experimental Station, Wilmington, Delaware 19880-0328.
Received January 15, 1990

Abstract: The reaction of tris(dimethylamino)sulfonium trimethyldifluorosilicate with fluorinated macrocyclic ether **3** provides a novel fluoride ion nesting complex **4**. X-ray crystal structure analysis shows that the central fluoride is held within the chiral cavity (C_2 symmetry) by interaction with four CH_2 groups. The nearest tris(dimethylamino)sulfonium (TAS) cation serves as a lid for the complex anion. The 18-membered ring undergoes substantial conformational change to accommodate the fluoride ion guest. NMR spectra show that the central fluoride is tightly bound. Multiple pathways for enantiomerization are found, and the preferred pathway depends upon the temperature. Measured rate constants for the pair-wise exchange of diastereotopic nuclei (-95 °C to -70 °C) give activation parameters for one "normal" enantiomerization process: $\Delta G^\ddagger$ = 9.8 kcal/mol, $\Delta H^\ddagger$ = 9.1 kcal/mol, $\Delta S^\ddagger$ = -3.7 eu. At lower temperatures, anti-Arrhenius behavior is observed for another conformational process in which the rate of exchange of geminally coupled nuclei increases as the temperature decreases. Ab initio calculations on a model of the anion complex indicate a minimum-energy geometry similar to that observed in the crystal structure of the salt.

Introduction

Noncovalent or supramolecular chemistry is an exceptionally active area of research.[2-5] Despite this activity, synthetic anion-binding substances are rather rare,[6-9] and studies of cooperative binding behavior involving highly fluorinated hosts have not been reported. Whereas a variety of fluorinated, anionic complexes which might be considered in host/guest terms have been reported,[10-14] these complexes involve predominantly covalent in-

(1) Dedicated to Professor Kurt Mislow.

(2) (a) Pederson, C. J. *Angew. Chem., Int. Ed. Engl.* **1988**, *27*, 1021. (b) Cram, D. J. *Science* **1988**, *240*, 760. (c) Lehn, J.-M. *Angew. Chem., Int. Ed. Engl.* **1988**, *27*, 90.

(3) (a) Izatt, R. M., Christensen, J. J., Ed. Synthesis of Macrocycles. The Design of Selective Complexing Agents. In *Progress in Macrocyclic Chemistry*; John Wiley and Sons: New York, 1987; Vol. 3. (b) Atwood, J. L.; Davies, J. E. D.; MacNicol, D. D. *Inclusion Compounds*; Academic Press: London, 1984; Vols. 1 and 2. (c) Vogtle, F., Weber, E., Ed. *Host-Guest Complex Chemistry/Macrocycles*; Springer-Verlag: Berlin, 1985.

(4) (a) Curtiss, L. A.; Blander, M. *Chem. Rev.* **1988**, *88*, 827. (b) Nesbitt, D. J. *Chem. Rev.* **1988**, *88*, 843. (c) Hobza, P.; Zahradnik, R. *Chem. Rev.* **1988**, *88*, 871. (d) Reed, A. E.; Curtiss, L. A.; Weinhold, F. *Chem. Rev.* **1988**, *88*, 899.

(5) (a) Conformational analysis of crown ether/cation complexes has received considerable attention, and the work reported here bears a formal resemblence to some of these studies. We deal with a reasonably robust complex which is characterized by unusual functionalities and by bizarre dynamic properties. For a review of previous NMR studies, see: Sutherland, I. O. Guest-Host Chemistry and Conformational Analysis. In *Methods in Stereochemical Analysis*; Vol. 6, Marchand, A. P., Ed.; VCH Pubishers, Inc.: Deerfield Beach, FL 1986; Vol. 6. (b) Stauffer, D. A.; Dougherty, D. A. *Tetrahedron Lett.* **1988**, *29*, 6039.

(6) Park, C. H.; Simmons, H. E. *J. Am. Chem. Soc.* **1968**, *90*, 2431.

(7) (a) Graf, E.; Lehn, J.-M. *J. Am. Chem. Soc.* **1976**, *98*, 6403. (b) Lehn, J.-M.; Sonveaux, E.; Willard, A. K. *J. Am. Chem. Soc.* **1978**, *100*, 4914. (c) Kintzinger, J.-P.; Lehn, J.-M.; Kauffmann, E.; Dye, J. L.; Popov, A. I. *J. Am. Chem. Soc.* **1983**, *105*, 7549. (d) Motekaitis, R. J.; Martell, A. E.; Dietrich, B.; Lehn, J.-M. *Inorg. Chem.* **1984**, *23*, 1588. (e) Hosseini, M. W.; Lehn, J.-M. *Helv. Chim. Acta* **1988**, *71*, 749. (f) Hosseini, M. W.; Blacker, A. J.; Lehn, J.-M. *J. Chem. Soc., Chem. Commun.* **1988**, *596*. (g) Fujita, T.; Lehn, J.-M. *Tetrahedron Lett.* **1988**, *29*, 1709. (h) Dietrich, B.; Guilhem, J.; Lehn, J.-M.; Pascard, C.; Sonveaux, E. *Helv. Chim. Acta* **1984**, *67*, 91. (i) Dietrich, B.; Lehn, J.-M.; Guilhem, J.; Pascard, C. *Tetrahedron Lett.* **1989**, 4125.

(8) (a) Bell, R. A.; Christoph, G. G.; Fronczek, F. R.; Marsh, R. E. *Science* **1975**, *190*, 151. (b) Metz, B.; Rosalky, J. M.; Weiss, R. *J. Chem. Soc., Chem. Commun.* **1976**, 533.

(9) (a) Newcomb, M.; Blanda, M. T. *Tetrahedron Lett.* **1988**, *29*, 4261. (b) Jung, M. E.; Xia, H. *Tetrahedron Lett.* **1988**, *29*, 297. (c) Katz, H. E. *J. Org. Chem.* **1985**, *50*, 5027. (d) Wuest, J. D.; Zacharie, B. *J. Am. Chem. Soc.* **1987**, *109*, 4714. (e) Muller, G.; Riede, J.; Schmidtchen, F. P. *Angew. Chem., Int. Ed. Engl.* **1988**, *27*, 1516.

(10) (a) Farnham, W. B.; Dixon, D. A.; Calabrese, J. C. *J. Am. Chem. Soc.* **1988**, *110*, 8453. (b) Farnham, W. B.; Smart, B. E.; Middleton, W. J.; Calabrese, J. C.; Dixon, D. A. *J. Am. Chem. Soc.* **1985**, *107*, 4565.

(11) Hiraoka, K.; Mizuse, S.; Yamabe, S. *J. Chem. Phys.* **1987**, *86*, 4102.

(12) Perfluorinated crown ethers have been prepared, but their interaction with potential guest molecules or ions is apparently minimal. See: Lin, W.-H.; Bailey, W. I., Jr.; Lagow, R. L. *J. Chem. Soc., Chem. Commun.* **1985**, 1350.

0002-7863/90/1512-7707$02.50/0

teractions between the neutral and anionic addends. In the gas phase, however, it has been suggested that F^- can bind to hydrogens by strong hydrogen bonds.[14] In addition, mass spectrometric techniques have identified a number of complexes which involve hydrogen bonding as the means for binding fluoride ion. Although the binding energies of some of these complexes may be in the range of interest, the kinds of shape/size selectivity and geometric elegance expected of host/guest complexes have been lacking.

Our new silicon-mediated synthesis of highly fluorinated vinyl ether polymers[15] has provided a family of related macrocyclic ethers. One of these macrocycles exhibits remarkable binding properties for fluoride ion. We report here a range of studies on the host and complex including synthesis, structure, dynamic properties, and theoretical modeling. The complex has interesting dynamical behavior and at least one process exhibits anti-Arrhenius behavior.

Experimental Section

General Remarks. ^{19}F NMR spectra were recorded on a Nicolet NT-200 spectrometer at 188.2 MHz and chemical shifts were recorded in ppm from $CFCl_3$. Selective inversion/recovery experiments were carried out by using a Nicolet NT-360 spectrometer at 339.34 MHz. ^1H NMR spectra were recorded on Nicolet NT-360 and GE QE-300 spectrometers, and chemical shifts are recorded in ppm from $(CH_3)_4Si$. Gas chromatographic analyses were carried out by using a Hewlett-Packard 5890 instrument with 25 m × 0.2 mm HP1 cross-linked methyl silicone capillary column, operating at 60–250 °C. Mass spectral data were obtained by using VG 7070-HS (with Varian Vista 6000 GC), VG 70-SE (with HP 5790 GC), or VG ZAB-2F (high resolution) instruments.

Cesium fluoride was dried at 400 °C in a stream of dry nitrogen. Solvents with minimum water concentration are required for preparation and manipulation of the fluoride complex reported here. Tetrahydrofuran, dimethoxyethane, and diethyl ether were distilled from sodium/benzophenone and stored over activated molecular sieves. All reactions were carried out in an atmosphere of dry nitrogen, and manipulations of the fluoride complex were performed in a Vacuum Atmospheres drybox.

Synthesis. Preparation of Bis(trimethylsilyl) Ether 1. A sample of 2,2,3,3,4,4-hexafluoro-1,5-pentanediol (23.1 g, 109 mmol) was treated with hexamethyldisilazane (20.6 g, 125 mmol) and heated slowly to 50 °C. After gas evolution started, the mixture was heated at 80 °C for 1.0 h. Kugelrohr distillation gave 37.1 g of colorless oil (96%), bp 45–48 °C (0.1 mm). GC analysis showed >99.8% purity. ^{19}F NMR ($CDCl_3$/F11): −122.4 (m, 4 F), −126.4 (s, 2 F). ^1H NMR ($CDCl_3$): 4.08 (m, 4 H), 0.20 (s, 18 H).

Preparation of Bis(2,3,3,4,4-pentafluorocyclobutenyl) Ether 2. A solution of bis (trimethylsilyl) ether **1** (17.8 g, 49.9 mmol) in glyme (125 mL) at −50 °C was treated with perfluorocyclobutene (32.2 g, 20.2 mL, 200 mmol; *Caution*: toxic) and cesium fluoride (0.5 g). The mixture was warmed to 0 °C and stirred for 2.5 h. It was then allowed to warm slowly to 25 °C over 18 h. Excess hexafluorocyclobutene was transferred under vacuum to a trap for recovery. The remaining mixture was diluted with ether, washed with water, dried, evaporated, and Kugelrohr distilled to give 21.8 g (88% yield) colorless oil, bp 60 °C (0.1 mm). GC analysis showed 99.6% purity. ^{19}F NMR (THF-d_8): −117.15 (m, 4 F), −119.8 (m, 4 F), −120.7 (m, 4 F), −125.3 (s, 2 F), −138.55 (m, 2 F(vinyl)). ^1H NMR (THF-d_8): 5.00 (m).

Preparation of Macrocycle 3. A solution of bis(vinyl) ether **2** (4.96 g, 10.0 mmol) and bis(trimethylsilyl) ether **1** (3.56 g, 10.0 mmol) in glyme (500 mL) at −20 °C was treated with cesium fluoride (200 mg). The mixture was warmed slowly to 25 °C and stirred for 18 h. Ether (200 mL) was added and the mixture was filtered, evaporated, and Kugelrohr distilled to provide 3.48 g of white solid, bp 124–156 °C (0.1 mm). GC analysis showed two major products in a 3.7/1 ratio. GC/MS showed both components with parent ion of m/z = 668. Recrystallization from ether gave 2.88 g which contained ca. 3% of the minor isomer (which was not characterized further). A second recrystallization gave 2.27 g, mp = 122–123 °C with purity >99.8%. Crystals of **3** suitable for X-ray diffraction analysis were grown by slow cooling of an ether solution. ^{19}F NMR (THF-d_8): −114.53 (s, 8 F), −120.6 (m, 8 F, CH_2CF_2), −125.06 (s, 4 F); line shapes were unchanged to −70 °C. ^1H NMR: 4.85 (m) (line shape was independent of temperature to −85 °C).

Table I. X-ray Crystallography Parameters for **3–5**

parameter	3	4	5
formula	$F_{20}O_4C_8H_{18}$	$SF_{21}O_4N_3C_{24}H_{26}$	$SF_{21}O_4N_3C_{33}H_{38}$
formula wt	668.26	851.55	971.75
space group	$P2_1/c$ (14)	$P2_1/n$ (14)	$P\bar{1}$ (2)
a, Å	5.345 (3)	9.742 (3)	16.521 (4)
b, Å	9.534 (2)	18.906 (5)	20.376 (7)
c, Å	21.390 (3)	18.096 (3)	12.435 (5)
α, deg	90	90	107.51 (3)
β, deg	90.79 (3)	101.54 (2)	89.85 (3)
γ, deg	90	90	93.14 (2)
V, Å^3	1089.9	3265.6	3985.6
Z	2	4	4
ρ(calc), g cm^{-3}	2.036	1.732	1.619
crystal dimension, mm	0.14 × 0.09 × 0.58	0.30 × 0.14 × 0.38	0.40 × 0.40 × 0.45
temperature, °C	−70	−100	−100
absorption coefficient, cm^{-1}	2.42	2.46	2.12
2θ	$1.9 < 2\theta < 55$	$4.3 < 2\theta < 54.0$	$4.2 < 2\theta < 48.0$
total data	2745	7816	13127
data $I > 3\sigma(I)$	1410	2966	7053
parameters	206	582	1117
R	0.035	0.042	0.062
R_w	0.034	0.032	0.053
residual ρ max e/Å^3	0.34	0.29	0.68

Preparation of Tris(dimethylamino)sulfonium (TAS) Fluoride Complex 4. A solution of macrocycle **3** (446 mg, 0.67 mmol) in THF (3 mL) was added to a mixture of TAS trimethyldifluorosilicate[16] (184 mg, 0.67 mmol) and THF (5 mL). The resulting colorless solution was evaporated at 1 mmHg to give 570 mg of white solid, mp 108–110 °C dec. The solid was taken up in ether (5 mL), filtered to remove traces of insoluble material, and cooled at −25 °C. Petroleum ether (0.8 mL) was added to enhance recovery of the white crystals. The supernatant was removed by pipet and solid was dried in vacuo. The melting (decomposition) point was unchanged. Crystals of **4** suitable for X-ray diffraction analysis were obtained by cooling an ether solution at −25 °C in an atmosphere of dry nitrogen. ^1H NMR (THF-d_8, 25 °C): 6.05 (br m, $w_{1/2}$ = 43 Hz, 8 H), 2.96 (s, 18 H). ^{19}F NMR (THF-d_8, 25 °C): −76.0 (br s, 1 F), −117.10 (s, 8 F), −123.67 (s, 8 F), −131.1 (s, 4 F).

Preparation of Tris(piperidino)sulfonium Fluoride Complex 5. A solution of macrocycle **3** (668 mg, 1.0 mmol) in THF (4 mL) was added to a solution of tris(piperidino)sulfonium trimethyldifluorosilicate (396 mg, 1.0 mmol) in THF (4 mL). The solution was evaporated at 1 mm to provide 975 mg of solid which was taken up in a minimal volume of ether, treated with ca. one fifth volume of petroleum ether, and cooled at −25 °C. There was obtained ca. 900 mg of crystals, mp = 106–108 °C dec. Crystals of **5** suitable for X-ray diffraction analysis were produced by cooling a solution of **5** in 1-chlorobutane/petroleum ether at −25 °C. ^1H NMR (THF-d_8, 25 °C): 6.05 (br m, 8 H), 3.33 (s, 12 H), 1.69 (s, 18 H). ^{19}F NMR (THF-d_8, 25 °C): −76.8 (s, 1 F), −116.87 (s, 8 F), −123.40 (s, 8 F), −131.06 (s, 4 F).

Preparation of Macrocycle 6. A solution of 1,5-pentanediol bis(pentafluorocyclobutenyl) ether (4.5 g, 11.6 mmol) and 1,5-pentanediol bis(trimethylsilyl) ether (2.88 g, 11.6 mmol) in glyme (400 mL) at 0 °C was treated with tris(piperidino)sulfonium trimethyldifluorosilicate (100 mg, 0.25 mmol). The solution was warmed slowly to 25 °C and stirred for 24 h. Solvent was removed under reduced pressure, and the residue was taken up in ether (200 mL), washed with water, dried ($MgSO_4$), and evaporated to give 5.5 g of partially crystalline residue. Kugelrohr distillation afforded 2.2 g of material bp 150–160 °C (0.1 mm) which was contaminated with decomposition products. Trituration with cold ether and recrystallization (ether) gave 0.6 g of white solid, mp 110 °C, which was homogeneous by GC. ^1H NMR (THF-d_8): 4.20 (t, J = 6.5 Hz, 8 H), 1.80 (m, 8 H), 1.52 (m, 4 H). ^{19}F NMR (THF-d_8): −113.01 (s). GC/MS showed one component with M^+ of m/z = 452.1219 (calcd for $C_{18}H_{20}F_8O_4$ 452.12338).

^1H NMR Line-Shape Simulation for Intermolecular Fluoride Exchange. The ^1H NMR line shape of complex **4** alone undergoes a large change between −80 and +20 °C. To simplify the analysis, values of chemical shifts and T_2 for the complex **4** were selected in order to match the

(13) Wuest, J. D.; Zacharie, B. *J. Am. Chem. Soc.* **1987**, *109*, 4714.
(14) (a) Larson, J. W.; McMahon, T. B. *J. Am. Chem. Soc.* **1983**, *105*, 2944. (b) Larson, J. W.; McMahon, T. B. *J. Phys. Chem.* **1984**, *88*, 1083. (c) Larson, J. W.; McMahon, T. B. *J. Am. Chem. Soc.* **1985**, *107*, 766. (d) Larson, J. W.; McMahon, T. B. *J. Am. Chem. Soc.* **1982**, *104*, 5848.
(15) Farnham, W. B., to be submitted for publication.
(16) Middleton, W. J. (to Du Pont) U.S. Patent 3 940 402. Middleton, W. J. *Org. Synth.* **1985**, *64*, 221.

observed broadened spectrum for the complex alone (−30 to + 10 °C). The resulting values were then used in simulating (DNMR3) the two-site exchange involving complex **4** and host **3**.

Crystal Structure Analysis. The crystal structure structure data are summarized in Table I. Data for **3** were collected on an Enraf-Nonius CAD4 diffractometer equipped with a graphite monochromator. Data for **4** and **5** were collected on a Syntex R3 diffractometer equipped with a graphite monochromator using Mo Kα radiation. For **3**, two standards were collected 37 times with a 3% fluctuation and a 4.5% variation in azimuthal scan. For **4**, three standards were collected 41 times with a 2% fluctuation and a 2.5% variation in azimuthal scan. For **5**, three standards were collected 72 times with a 4% variation in azimuthal scan. The data for **5** were adjusted for a 3% decrease in intensity. No absorption corrections were made for **3**, **4**, or **5**.

The structures for **3** and **4** were solved by direct methods (MULTAN)[17a] by using full-matrix least squares refinement. Scattering factors were from the International Tables for X-ray Crystallography, Vol. IV.[17b] All hydrogens were refined isotropically; other atoms, anisotropically. A biweighting scheme proportional to $[\sigma^2(I) + 0.009I^2]^{1/2}$ was used. The asymmetric unit for **3** consists of half the molecule related via the inversion center at [0.5, 0.5, 0.5].

The structure for **5** was also solved by direct methods by using full-matrix least-squares refinement. However, finding a suitable single crystal for this study proved somewhat difficult; all of the crystals examined appeared to be multiple. The crystal which was used for data collection had reasonable ω profiles but, even so, one weak peak was found by the search/center routine which could not be indexed. The cell was determined to be triclinic, although it could be transformed into a cell which was nearly C-centered monoclinic; the transformed cell parameters are a = 38.864 Å, b = 12.435 Å, c = 16.521 Å, α = 90.15°, β = 93.24°, and γ = 90.26°. The matrix for this transformation is (0,2,1,0,0,1,1,0,0). The intensity data, however, showed no twofold or mirror symmetry. It is not clear whether the pseudomonoclinic cell might contribute to a twinning mechanism which makes it difficult to grow good single crystals with clean ω profiles. Although the structure solved and refined reasonably well, the R valves remained higher than expected for a well-determined structure. Furthermore, attempts to refine even the 16 hydrogen atoms of the cyclic ethers (two independent molecules per unit cell) resulted in widely disparate C–H bond lengths: 0.8–1.2 Å. Eventually, all of the hydrogen atoms were idealized, C–H = 0.95 Å, with thermal parameters set equal to 1 plus the isotropic value of the carbon atom to which each was attached. Biweights were used to eliminate some of the reflections which were seriously in error; observed F's were consistently greater than calculated F's suggesting contributions from secondary crystallites. The largest peak in the final difference map, 0.68 e Å^{-3}, was located near C(85). Several other peaks in the range 0.4 to 0.5 e Å^{-3} were found near the sulfur atoms and near the $C_5H_{10}N$ rings; they did not appear to be chemically meaningful (i.e., the rings did not appear to be disordered).

Theoretical. Ab initio molecular orbital calculations on a model for the host **7** and for the complex **8** were performed with the STO-3G basis set.[18] The model compound is identical with the actual compound except that hydrogens were substituted for fluorines on the four-membered rings. All calculations were done with the program GRADSCF[19] on a CRAY X-MP/24 computer. The X-ray geometries were approximately symmetrized to the ideal symmetry for C_i for the host and C_2 for the complex. An additional C_2 conformer of the host obtained by removing the fluoride from the complex was also studied. The geometries were optimized by using gradient techniques.[20] Force fields were calculated analytically.[21]

Results

The polycondensation reaction of difunctional silyl ethers with fluorinated olefins gives partially fluorinated vinyl ether polymers along with cyclic oligomers (eq 1).[15] Modification of reaction conditions provides surprisingly good (ca. 50%) yields of cyclic dimers (eq 2). Macrocycle **3** exhibits unusual binding properties: treatment of **3** with an equimolar quantity of tris(dimethylamino)sulfonium (TAS) trimethyldifluorosiliconate[16] affords a quantitative yield of the fluoride adduct **4** (eq 3).

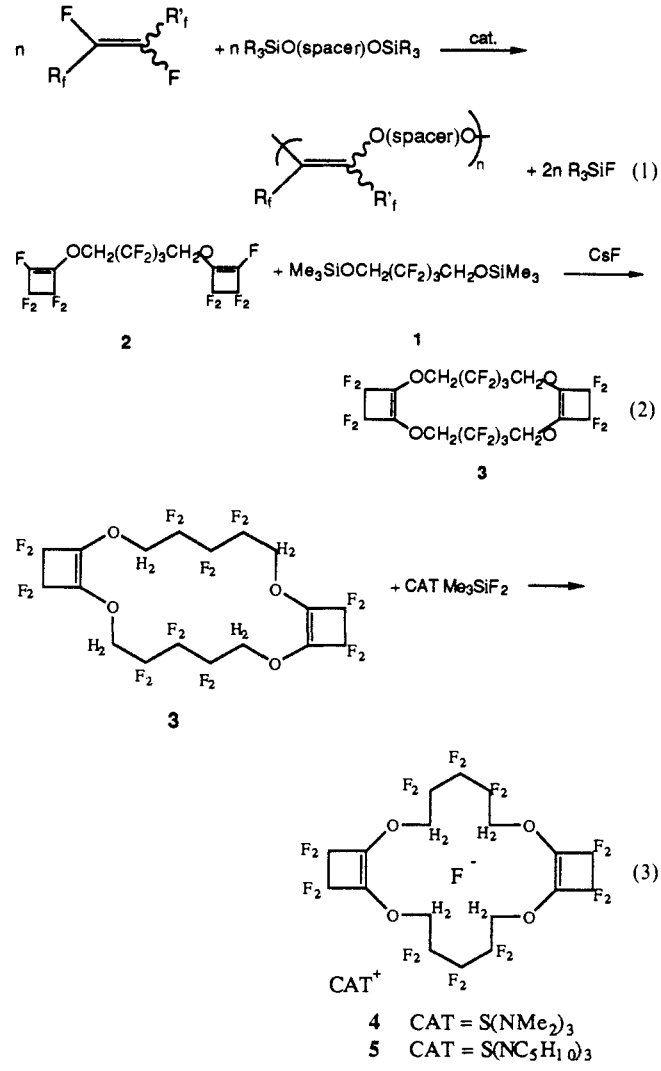

4 CAT = $S(NMe_2)_3$

5 CAT = $S(NC_5H_{10})_3$

Since there was no precedent for fluoride binding by neutral species with the functionalities represented by macrocycle **3**, an X-ray crystal structure analysis was undertaken. The adduct **4** takes the form of a "nesting"[2] complex in which the central fluoride lies within a twisted, cup-shaped cavity formed by the 18-membered macrocyclic ether as shown in Figure 1a,b. Although the

Table II. Molecular Parameters for the F^- Cavity[a]

parameter	4[b]	5[b]	5'[b]	8[c]
F21–H5′	2.08	2.07	2.12	1.434
F21–H9′	2.06	2.06	2.09	1.397
F21–H14′	2.10	2.08	2.11	1.437
F21–H19′	1.94	2.09	2.10	1.415
C5–H5′–F21	157	159	155	172.8
C9–C9′–F21	156	163	160	177.0
C14–H14′–F21	153	149	148	172.9
C18–H18′–F21	165	165	161	177.3
H5′–F21–F14′	143	142	144	152.1
H9′–F21–H18′	112	114	112	155.4
F5′–F21–H9′	81	72	72	85.7
H9′–F21–H14′	77	92	90	88.7
H14′–F21–H18′	85	71	72	85.2
H18′–F21–H5′	76	85	85	88.6

[a] Bond distances in angstroms. Bond angles in degrees. [b] From X-ray crystal data. [c] Optimized structure from ab initio molecular orbital theory.

(17) (a) Main, P.; Lessinger, L.; Woolfson, M. M.; Germain, G.; Declarz, J. P. MULTAN; Universities of York and Louvain: York, England and Louvain-la-Neuve, Belgium, 1978. (b) *International Tables for X-ray Crystallography*; Kynoch Press: Birmingham, England, 1974; Vol. IV.

(18) Hehre, W. J.; Stewart, R. F.; Pople, J. A. *J. Chem. Phys.* **1969**, *51*, 2657.

(19) GRADSCF is an ab initio gradient program system designed and written by A. Komornicki at Polyatomics Research.

(20) (a) Komornicki, A.; Ishida, K.; Morokuma, K.; Ditchfield, R.; Conrad, M. *Chem. Phys. Lett.* **1977**, *45*, 595. (b) McIver, J. W., Jr.; Komornicki, A. *Chem. Phys. Lett.* **1971**, *10*, 303. (c) Pulay, P. In *Applications of Electronic Structure Theory*; Schaefer, H. F., II, Ed.; Plenum Press: New York, 1977; p 153.

(21) (a) King, H. F.; Komornicki, A. In *Geometrical Derivatives of Energy Surfaces and Molecular Properties*; Jorgenson, P., Simons, J., Eds.; NATO Advanced Studies Institute Series C166; D. Reidel: Dordrecht, 1986; p 207. (b) King, H. F.; Komornicki, A. *J. Chem. Phys.* **1986**, *84*, 5645.

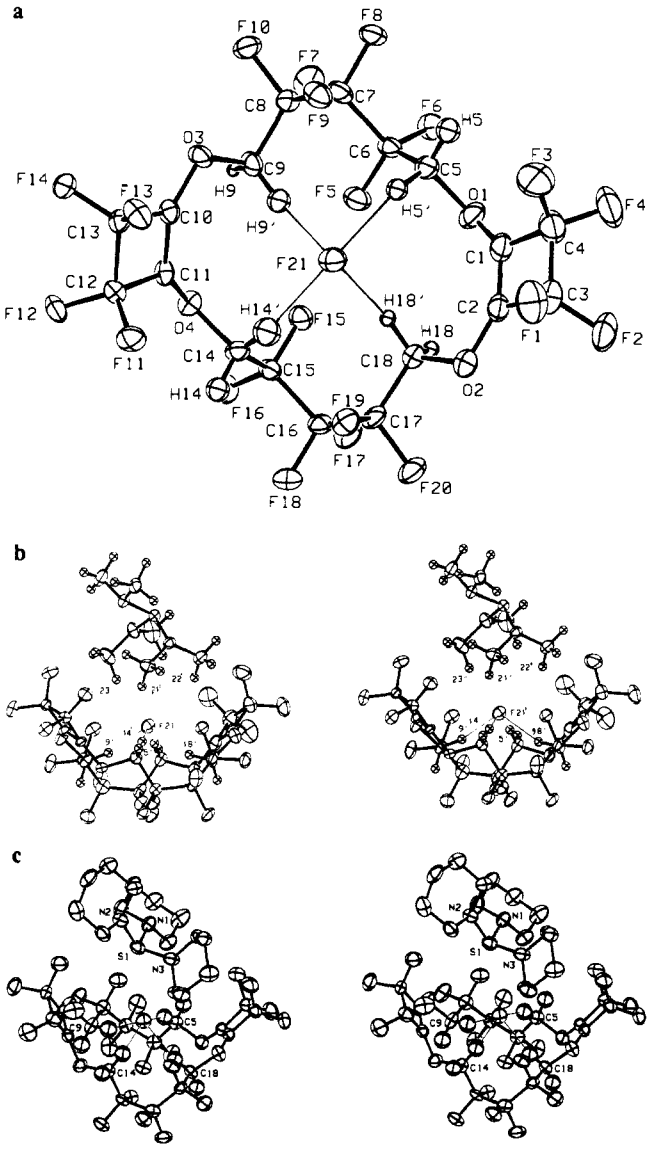

Figure 1. (a) X-ray crystal structure of **4**. Only the anion is shown. Note the formation of the nest and that the F^- is held by H-bonds. (b) X-ray crystal structure of **4**, view perpendicular to C_2 axis showing anion and cation. (c) X-ray crystal structure of **5**, view comparable to (b).

anion complex does not have crystallographic symmetry, it has approximately C_2 symmetry. The central fluoride is bonded by its interaction with four hydrogens[22] characterized by H–F distances of 1.94–2.10 Å and F–H–C angles of 158°. Table II contains the geometrical parameters related to the binding of the fluoride in the cavity. The remaining bond distances are given in Table III. The C–H bond distances are foreshortened as typically found in structures determined by X-ray analysis. We thus expect that the actual H–F^- bond distances are shorter than the ones given by the X-ray analysis. The nearest TAS cation hovers above the "nest", in order to maximize the electrostatic stabilization. Three methyl group hydrogens from the TAS cation are reasonably close to the fluoride (H–F = 2.33–2.73 Å). These F–H distances are significantly longer than the F(21)–H distances in the macrocyclic complex. All geometric attributes of the TAS

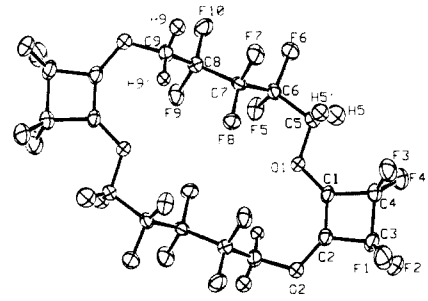

Figure 2. X-ray crystal structure of **3**. Note the extended open structure.

cation are perfectly normal for this species.[23] The "coordination" geometry at the central fluoride is not tetrahedral. In fact, the four nearest bonding neighbors are located in the same hemisphere. The observed structure is a balance between macrocycle conformational constraints and coordination requirements of the guest fluoride.[24-27]

Because of the close interactions of the TAS methyl protons with the F^-, a different sulfonium cation was selected in order to test the importance of electrostatic interactions of the protons on the cation with the F^-. The structure of complex **5** (Figure 1c) consists of two ion pairs which have virtually identical conformations. The conformations of the two anionic complexes for **5** are nearly superimposable on that of the complex **4**, and we can conclude that neither shape nor specific orientation of the cation has any effect upon the geometry of the anion. The H–F^- bond distances in the complex are somewhat longer in **5** than in **4** ranging between 2.06 and 2.12 Å. Part of this difference is accounted for by the shorter C–H bond distances (fixed at 0.95 Å) in **5**. In **5**, the contacts between the central fluoride and the cation are quite long, and the apex of the SN_3 pyramid points toward the interior of the cup-shaped anion. The most obvious difference between structures **4** and **5** is the orientation of the SN_3 pyramid with respect to the idealized C_2 axis of the anion complex. Whereas the packing arrangement in **4** favors $N(CH_3)_2$ groups as elements of closest approach to the central fluoride, the piperidinyl rings in **5** are more distant and the sulfur atom is oriented closer to the central fluoride. The closest atoms in the cation to the fluoride in **5** are still protons from the CH_2 groups in the piperidinyl rings. The shortest distances now are 2.76 and 2.77 Å for one ion pair and 2.79 and 2.92 Å for the other ion pair.

Crystal structure analysis of the free macrocycle **3** reveals a different geometry, as shown in Figure 2. The large ring system is extended rather than cup-shaped and is achiral (C_i). Using the center of symmetry within the large ring as a point of reference, there are two oxygen atoms (O_1) "pointing" toward the center which are adjacent to CH_2's with protons directed away from the center. The other pair of oxygen atoms (O_2) are "pointing" away

(22) Hydrogen bonding involving partially fluorinated alkanes and various donor solvents has been studied. See: Creswell, C. J.; Allred, A. L. *J. Am. Chem. Soc.* **1963**, *85*, 1723. Andersen, D. L.; Smith, R. A.; Myers, D. B.; Alley, S. K.; Williamson, A. G.; Scott, R. L. *J. Phys. Chem.* **1962**, *66*, 621. Alley, S. K.; Scott, R. L. *J. Phys. Chem.* **1963**, *67*, 1182. We have found no reference describing F^- binding by such molecules. Hydrogen bonding frequently plays a role in the organization of host/guest systems. For recent examples and leading references, see: Chang, S.-K.; Hamilton, A. D. *J. Am. Chem. Soc.* **1988**, *110*, 1318. Kelly, T. R.; Maguire, M. P. *J. Am. Chem. Soc.* **1987**, *109*, 6549. Reference 9e.

(23) Farnham, W. B.; Dixon, D. A.; Middleton, W. J.; Calabrese, J. C.; Harlow, R. L.; Whitney, J. F.; Jones, G. A.; Guggenberger, L. J. *J. Am. Chem. Soc.* **1987**, *109*, 476.

(24) The location of nearest neighbor atoms with respect to an "F^-" center appears to be rather variable. Geometries for two-coordinate examples range from near linear or linear[10] to severely bent.[25] Four-coordinate examples are tetrahedral (e.g., $F^-{\cdot}4H_2O$), although distortions from a tetrahedral geometry are accommodated.[26] The crystal structure of $KF{\cdot}4H_2O$ contains both K^+ and F^- ions surrounded by octahedra of oxygen atoms.[27] Although H's were not located with precision, F^- is involved in six H-bonding interactions. The crystal structure of $NH4^+$ F^-, on the other hand, contains tetrahedrally coordinated fluoride ion (ref 27, p 222). The question of F^- anion coordination geometry in the context of anion cryptate complexes has been addressed by Lehn and co-workers.[7h,7i] In these cases, either a distorted tetrahedral or quasitrigonal prismatic coordination geometry was preferred, depending on the size of the cavity.

(25) (a) Kralingen, C. G. van; Reedijk, J. *J. Chem. Soc., Chem. Commun.* **1976**, 533. (b) Emsley, J.; Arif, M.; Bates, P. A.; Hursthouse, M. B. *J. Chem. Soc.; Chem. Commun.* **1989**, 738.

(26) Emsley, J.; Arif, M.; Bates, P. A.; Hursthouse, M. B. *J. Chem. Soc., Chem. Commun.* **1988**, 1387. See also Carmona, C.; Eaton, G.; Symons, M. C. R. *J. Chem. Soc., Chem. Commun.* **1987**, 873.

(27) Hamilton, W. C.; Ibers, J. A. *Hydrogen Bonding in Solids*; W. A. Benjamin, Inc.: New York, 1968; p 216. See: Beurskens; Jeffrey *J. Chem. Phys.* **1964**, *41*, 917.

Table III. Bond Distances, Å

	host			complex			
		calcd		TAS salt	TPS salt		calcd
parameter	**3**	**7**	**7′**	**4**	**5**	**5′**	**8**
F1(H)-C3	1.359 ± 3	1.089	1.089	1.360 ± 5	1.355 ± 6	1.356 ± 6	1.088
F2(H)-C3	1.357 ± 3	1.089	1.089	1.345 ± 5	1.343 ± 6	1.361 ± 6	1.089
F3(H)-C4	1.361 ± 3	1.088	1.089	1.369 ± 5	1.366 ± 6	1.361 ± 6	1.090
F4(H)-C4	1.357 ± 3	1.089	1.090	1.358 ± 5	1.355 ± 6	1.364 ± 6	1.089
F5-C6	1.352 ± 3	1.377	1.379	1.354 ± 4	1.354 ± 6	1.361 ± 7	1.380
F6-C6	1.356 ± 3	1.380	1.380	1.360 ± 4	1.364 ± 6	1.362 ± 6	1.384
F7-C7	1.357 ± 3	1.380	1.378	1.348 ± 4	1.333 ± 5	1.358 ± 6	1.383
F8-C7	1.347 ± 3	1.375	1.379	1.357 ± 4	1.361 ± 6	1.324 ± 6	1.381
F9-C8	1.350 ± 3	1.377	1.379	1.363 ± 4	1.364 ± 6	1.355 ± 6	1.381
F10-C8	1.351 ± 3	1.378	1.379	1.364 ± 4	1.355 ± 6	1.350 ± 6	1.386
F11-C12				1.362 ± 4	1.347 ± 6	1.360 ± 6	
F12-C12				1.350 ± 4	1.351 ± 6	1.367 ± 6	
F13-C13				1.354 ± 4	1.350 ± 6	1.346 ± 6	
F14-C13				1.361 ± 4	1.372 ± 6	1.356 ± 6	
F15-C15				1.354 ± 4	1.348 ± 5	1.349 ± 6	
F16-C15				1.357 ± 4	1.363 ± 5	1.350 ± 6	
F17-C16				1.348 ± 4	1.352 ± 6	1.359 ± 6	
F18-C16				1.359 ± 4	1.360 ± 6	1.359 ± 6	
F19-C17				1.362 ± 4	1.355 ± 5	1.351 ± 6	
F20-C17				1.364 ± 4	1.340 ± 6	1.364 ± 6	
O1-C1	1.337 ± 3	1.397	1.395	1.363 ± 5	1.364 ± 6	1.343 ± 6	1.392
O1-C5	1.428 ± 3	1.435	1.439	1.439 ± 5	1.449 ± 6	1.433 ± 6	1.453
O2-C2	1.344 ± 3	1.387	1.385	1.344 ± 4	1.326 ± 6	1.332 ± 7	1.376
O2-C9a(18)	1.438 ± 3	1.437	1.438	1.442 ± 5	1.441 ± 6	1.448 ± 6	1.450
O3-C9				1.456 ± 5	1.449 ± 6	1.439 ± 6	
O3-C10				1.329 ± 4	1.347 ± 6	1.315 ± 6	
O4-C11				1.345 ± 4	1.360 ± 6	1.349 ± 6	
O4-C14				1.443 ± 5	1.449 ± 6	1.423 ± 6	
C1-C2	1.333 ± 4	1.326	1.325	1.324 ± 6	1.323 ± 7	1.324 ± 8	1.330
C1-C4	1.489 ± 4	1.530	1.533	1.478 ± 6	1.462 ± 7	1.474 ± 8	1.534
C2-C3	1.473 ± 4	1.526	1.528	1.497 ± 6	1.488 ± 8	1.485 ± 8	1.529
C3-C4	1.535 ± 4	1.563	1.562	1.536 ± 6	1.544 ± 8	1.529 ± 9	1.560
C5-C6	1.517 ± 4	1.573	1.570	1.501 ± 6	1.501 ± 7	1.495 ± 7	1.563
C6-C7	1.542 ± 4	1.604	1.606	1.529 ± 5	1.519 ± 7	1.531 ± 8	1.604
C7-C8	1.528 ± 4	1.604	1.607	1.542 ± 5	1.553 ± 7	1.552 ± 8	1.604
C8-C9	1.520 ± 4	1.575	1.569	1.492 ± 5	1.494 ± 7	1.502 ± 7	1.564
C10-C11				1.341 ± 5	1.306 ± 7	1.351 ± 7	
C10-C13				1.490 ± 5	1.470 ± 7	1.484 ± 7	
C11-C12				1.488 ± 5	1.488 ± 7	1.474 ± 7	
C12-C13				1.543 ± 5	1.532 ± 8	1.535 ± 8	
C14-C15				1.505 ± 5	1.485 ± 7	1.492 ± 7	
C15-C16				1.537 ± 5	1.540 ± 7	1.541 ± 8	
C16-C17				1.540 ± 5	1.545 ± 7	1.534 ± 8	
C17-C18				1.503 ± 5	1.507 ± 7	1.498 ± 8	
C5-H5	0.977 ± 29	1.096	1.096	0.957 ± 36			1.095
C5-H5′	0.979 ± 27	1.097	1.095	1.007 ± 35			1.147
C9-H9	0.932 ± 27	1.094	1.096	0.941 ± 31			1.095
C9-H9′	0.995 ± 26	1.094	1.093	1.003 ± 35			1.164
C14-H14				0.964 ± 36			
C14-H14′				0.971 ± 37			
C18-H18				0.882 ± 34			
C18-H18′				0.982 ± 33			

from the center and are adjacent to CH_2's with protons directed toward the interior portion of the ring.

Formation of the binding cavity for the central fluoride in complex **4** requires several bond rotations. This situation is similar to that found for many crown ethers and their cation complexes: the binding cavity is realized only in the presence of the guest.[2a] In order to see how the large ring system changes its conformation, we examined the torsion angles as shown in Table IV. Major changes occur at 10 bonds in going from **3** to **4**. The changes take anti orientations into gauche and vice versa. Except for the imposed geometric constraints, minimum-energy-framework torsional angles for these systems are probably near 180°, and torsions about only four bonds in the host, two C–O bonds and two C–C bonds, deviate from the optimal values. These nonoptimal bonds are changed to more favorable geometries in the complex, but the other two C–O bonds along with four C–C bonds become nonoptimal in the complex. The ring conformations of macrocycle **3** and complex **4** may be analyzed in terms of standard intraannular torsional angle descriptors.[28-30] These torsional angle descriptors which correspond to the enantiomer of **4** shown in Figure 1 are given in Table IV. It is evident that the constraints on the system ("fixed" CH_2 groups and double bonds) result in large differences between conformations of **4** and other 18-membered ring systems (e.g., cyclooctadecane, 18-crown-6 and its complexes). Each $-(CF_2)_3-$ segment in the complex defines a short helical array as shown by inspection of dihedral angles (e.g. $\angle F_6C_6C_7F_8$, $\angle F_8C_7C_8F_9$) in Figure 1. On the basis of our previous work on the conformations of unconstrained fluorocarbon chains,[31]

(28) Bucourt, R. The Torsional Angle Concept in Conformational Analysis. *Topics Stereochem.* **1974**, *8*, 159.
(29) Dale, J. Multistep Conformational Interconversion Mechanisms. *Topics Stereochem.* **1976**, *9*, 199.
(30) Anet, F. A. L.; Anet, R. In *Dynamic Nuclear Magnetic Resonance Spectroscopy*; Jackman, L. M., Cotton, F. A., Eds.; Academic Press: New York, 1975; Chapter 14.
(31) (a) Dixon, D. A.; Van-Catledge, F. A. *Int. J. Supercomputer Appl.* **1988**, *2*, No. 2, 62. (b) Dixon, D. A.; Farnham, W. B.; Capobianco, P. J. *Int. J. Supercomputer Appl.* **1990**, *4*, No. 2, 134.

Table IV. Intraannular Torsional Angles

location[a]	3	7	type[b]	7′	4	type[b]	8
C1-C2	-0.7	1.5	-	-5.0	-4.8	-	-3.1
O1-C1	175.2	172.6	a	125.4	111.0	g	88.8
C5-O1	177.0	-176.6	a	-172.0	-168.3	a	-179.0
C6-C5	78.4	76.7	g+	171.9	-176.4	a	-162.3
C7-C6	165.7	-163.1	a	-61.3	-54.9	g-	-40.7
C8-C7	-173.3	-169.5	a	-57.6	-51.3	g-	-50.2
C9-C8	-172.3	-176.3	a	-176.6	-172.6	a	-163.1
O3-C9	93.9	88.7	g+	-167.7	-168.7	a	-175.5
O3-C10	-8.7	3.1	-	-5.1	-10.1	-	-9.7
C11-C10					-3.1	-	
O4-C11					109.5	g	
C14-O4					-167.8	a	
C14-C15					-176.0	a	
C16-C15					-52.6	g-	
C17-C16					-55.0	g-	
C18-C17					-173.1	a	
O2-C18					-168.4	a	
O2-C2					-6.7	-	

[a] Only the central bond for the dihedral angle is listed. [b] Angle types for nearly eclipsed angles or dihedrals involving trigonal carbon atoms are omitted. a = anti; g = gauche.

we would expect the C–C torsions to be ca. 180° for a perfluoro-C_3 moiety, although longer chains do show a helical twist. The observed deviations can be attributed to either small amounts of ring strain or to the electronic effects of the $-CH_2-O-$ substituent.

Partial fluorination of the five-carbon segments between oxygen nuclei is a necessary condition for achieving a measureable degree of fluoride binding. Treatment of macrocycle **6** with TAS trimethyldifluorosilcate results in no detectable reaction under a variety of conditions. Substantial differences exist in the electronic

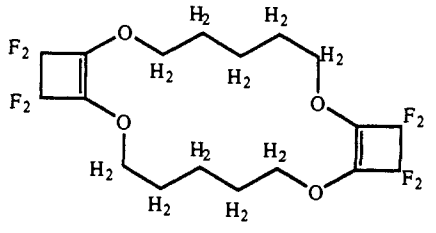

6

environment for the OCH_2 groups in macrocycles **3** and **6**. The lack of binding potential for **6** is also understandable in terms of the charge distribution for complex **4** (vide infra).

A cyclic array of special OCH_2 groups seems necessary for effective binding of fluoride ion. Linear structures which are otherwise similar to **3** [e.g., diene **9**] do not appear to form stable adducts when TAS trimethyldifluorosilicate is used as fluoride source.

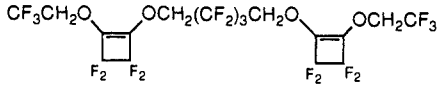

diene **9**

Although we have not made quantitative measurements of the fluoride affinity of macrocycle **3**, the identity of the fluoride ion donor used in eq 3 is clearly important. Treatment of macrocycle **3** with a representative perfluorinated carbanion, TAS 1,1,1,3,3,4,4,5,5,5-decafluoro-2-(trifluoromethyl)-2-pentanide (which transfers fluoride ion to other acceptors under similar conditions[10a]), does not lead to the formation of complex **4**.

Theoretical Models. In order to better understand the structure of the complex, we performed ab initio molecular orbital calculations on our model compound for the host (**7**), the complex (**8**) and on the host in the conformation (**7′**) that it has in the complex. Geometric parameters are given in Tables II–IV. There is overall good agreement between theory and experiment, considering the size of the basis set. The C–F, C–C and C–O bond distances are calculated to be too long by about 0.02–0.05 Å consistent with previous results.[31,32] The results for the bond angles and the

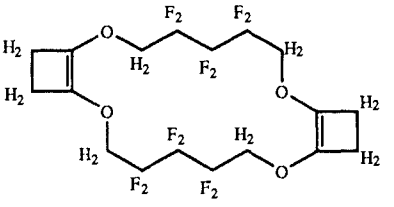

7

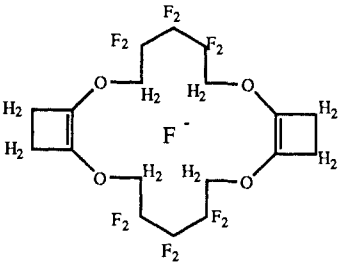

8

torsions demonstrate that we are able to properly model the general conformation of the ring.

In order to provide more information about the energetics of the formation of the complex **4**, we optimized the structure of **7** in the conformation required for the complex. This conformation (**7′**) is a true minimum on the potential energy surface as shown by a calculation of the force constants. As would be expected, it is higher in energy than the extended host conformation (**7**) by 3.1 kcal/mol. This result is consistent with the fact that there are two additional unfavorable C–C gauche interactions in **7′**. For butane,[31b] the gauche/trans energy difference is 0.7 kcal/mol and for perfluorobutane, the difference is 1.5 kcal/mol. The structure of **7′** is very similar to that of **7** with very small changes in bond lengths and bond angles. The differences in torsional angles for **7′** and **7** correspond to those discussed above for the host and complex structures. Further characterization of the structures is made by examining the low-frequency vibrational modes (<100 cm^{-1}), Structure **7′** (14 modes) is slightly more flexible than **7** (12 modes) consistent with the two extra unfavorable C–C torsions in **7′**.

The calculated structure (**8**) of the model complex reveals interesting differences with both the calculated structure of the neutral (**7′**) and the experimental structures (**4** and **5**). The C–F bond lengths in **8** show a small increase when compared to those of **7′**, consistent with a small amount of anionic hyperconjugation at these centers arising from the introduction of the fluoride ion. The calculated C–H bond distances for the hydrogens bonded to the F^- are all lengthened by 0.05 Å in comparison to the neutral. Although this increase may seem rather large, the structure of **4** shows a similar lengthening (Table III). The H–F^- bond distances calculated for **8** (ca. 1.40 Å) are significantly shorter than those observed in structures **4** and **5** (Table II). However, the reported experimental H–F^- distances would actually be shorter (i.e., in closer agreement) if better C–H bond lengths were used in the X-ray crystal structure analysis; for example, a more reasonable C–H distance of 1.12 Å leads to H–F^- distances ranging from 1.83 to 1.98 Å. Such differences are to be expected since, in the experimental structures, the cation can attract the fluoride ion away from the center of the cavity and thereby lengthen the H–F distances. Additionally, the calculated structure is of the gas-phase complex for which the degree of nesting is anticipated to be greater, and the use of a minimal basis set will also tend to make the nesting stronger since the F^- uses the basis functions in the complex to stabilize the negative charge.

The bond angles in **7′** do not change appreciably on complexation of F^-. The C–H–F^- bond angles are calculated to be slightly

(32) Dixon, D. A.; Fukunaga, T.; Smart, B. E. *J. Am. Chem. Soc.* **1986**, *108*, 4027. It should be pointed out that C–F distances as determined by X-ray diffraction techniques may be systematically shortened because of thermal motions of the F atoms.

Table V. Calculated Atomic Charges, e

atom	7	group[a]	7′	group[a]	8	group[a]
O1	-0.24		-0.24		-0.26	
O2	-0.23		-0.23		-0.25	
C1	0.07		0.06		0.07	
C2	0.09		0.10		0.10	
C3	-0.11	0.03	-0.10	0.04	-0.11	-0.01
C4	-0.11	0.01	-0.11	0.02	-0.11	-0.01
C5	-0.01	0.15	-0.01	0.15	0.08	0.13
C6	0.28	-0.01	0.27	-0.01	0.26	0.05
C7	0.25	-0.03	0.25	-0.03	0.24	-0.08
C8	0.27	-0.02	0.28	-0.01	0.26	-0.06
C9	-0.01	0.17	-0.01	0.17	-0.08	0.14
H1	0.07		0.07		0.05	
H2	0.07		0.07		0.05	
H3	0.06		0.06		0.05	
H4	0.06		0.07		0.05	
H5	0.08		0.08		0.04	
H5′	0.08		0.08		0.17	
H9	0.09		0.09		0.05	
H9′	0.09		0.09		0.17	
F5	-0.14		-0.14		-0.15	
F6	-0.15		-0.14		-0.16	
F7	-0.15		-0.14		-0.16	
F8	-0.13		-0.14		-0.16	
F9	-0.14		-0.15		-0.16	
F10	-0.15		-0.14		-0.16	
F⁻					-0.44	

[a] Group charges calculated by adding the charge on the H or F bonded to the carbon to the carbon charge.

more linear (175°) than is observed (157°). Similarly, the calculated H–F–H bond angles are around 154°, whereas in the observed structures one angle is near 143° and the other angle is smaller, near 113° (Table II). These angular differences are consistent with the fact that in the theoretical structure the fluoride ion is more tightly buried in the nest. We note that addition of the F^- to 7′ makes the complex significantly less flexible, with only 9 modes below 100 cm^{-1} in **8** compared to 14 modes for 7′. This loss of flexibility is relevant to the types of conformational dynamics described below.

The atomic charges are shown in Table V in order to provide a qualitative picture of the changes in charge density upon complexation. There are essentially no differences in the atomic charges between 7 and 7′. Although the charges do not differ, the change in conformation between 7 and 7′ leads to a dramatic difference in the dipole moment. The O atoms are quite negative in the host and the carbons bonded to the oxygens are positive. The charges for the remaining groups show them to be essentially neutral. The dipole moment in 7 is zero by symmetry (a slight deviation of the coordinates from perfect symmetry leads to a value of 0.07 D), but formation of the nest in 7′ leads to a large increase to 2.45 D. Complexation of the F^- leads to a distribution of the negative charge over the large ring. The negative charge on the central F is only 0.44 e. Although we are overestimating the amount of charge transfer due to the use of the Mulliken charges and the small basis set, there is clearly a significant amount of charge transfer. The hydrogens which bind the F^- become quite positive, and their geminal partners lose positive charge. The carbons in these CH_2 groups become significantly more negative, but the group charge gains only 0.02–0.03 e by comparison with 7′. The largest transfer of negative charge from the fluoride ion is to the CF_2 groups in the cavity; almost 0.05 e is transferred to each of the six CF_2 groups. The oxygens likewise gain a small amount of negative charge in **8**, and the CH_2 groups in the four-membered rings also gain 0.04–0.05 e. These results show that the negative charge that is transferred is dispersed over the whole host molecule.

Fluoride affinities of a wide range of molecules have been determined by ion cyclotron resonance spectroscopy.[14] The fluoride affinity is defined as $-\Delta H$ for reaction 4. Although we cannot

$$A + F^- \rightarrow AF^- \quad (4)$$

calculate absolute fluoride affinities due to the difficulties in calculating the electron affinity of F, we can calculate relative affinities and then convert these to absolute values by comparison to an absolute standard.[32] The fluoride affinity of CF_2O is well established as -42.6 kcal/mol. We thus calculate the energy of the reaction 5 to obtain a relative affinity. The binding of fluoride

$$CF_2O + 8 \rightarrow CF_3O^- + 7 \quad (5)$$

to 7 is 13.8 kcal/mol less favorable than binding to CF_2O, consistent with a hydrogen-bonding process for 7 and a covalent-bonding process for CF_2O. The reaction to form the less stable conformer is of course less exothermic, since 7′ is destabilized relative to 7. The energy of reaction 6 is -10.7 kcal/mol.

$$CF_2O + 8 \rightarrow CF_3O^- + 7' \quad (6)$$

The binding energy of F^- to simple ethers has been investigated by McMahon and Larsen using ICR techniques.[14] For example, the fluoride affinity of $(CHF_2)_2O$ is 36.0 kcal/mol and the affinity of CF_3OCF_2H is lower by 1.4 kcal/mol at 34.6 kcal/mol. These values are consistent with our estimated value of 28.8 kcal/mol for the fluoride affinity of **3**. In fact, McMahon has proposed a macrocyclic structure **10** similar to ours as a means for stabilizing anions.

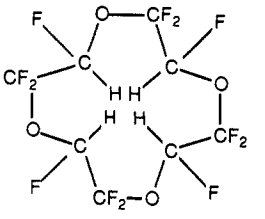

10

Table VI. Fluorine–Hydrogen Coupling Constants at -90 °C

fluorine	shift, ppm	coupling constants							
		H9′[b]	θ[a]	H9	θ[a]	H5′	θ[a]	H5	θ[a]
F21	-77.6	24		~0		22		~0	
F10	-126.6	28	170	~0	68	0		0	
F6	-126.0	0		0		26	172	~0	65
F5	-118.8	0		0		~0	54	~8[c]	178
F9	-117.1	~0[c]	54	~3	178	0		0	

[a] Dihedral angle θ(HCCF) from X-ray structure analysis. [b] Assignment of the lowest field ^1H signal to H9′ rather than H5′ is arbitrary. Vicinal HCCF coupling constants vary with dihedral angle and ^{19}F assignments are made accordingly. [c] Approximate value.

Spectroscopy and Dynamic Processes. Low-temperature NMR spectra of complex **4** are in complete accord with the X-ray structure as the only observable species in solution. The ^1H NMR spectrum (Figure 3) reveals four distinguishable H's: signals at lowest field (8.08 and 7.01) are assigned to those protons involved in binding the central fluoride (H9′, H18′ and H5′, H14′),[33] while the other two shifts (4.97 and 4.56), similar to that observed for protons in the free macrocycle **3**, are assigned to the geminal partners. A COSY experiment demonstrates that the geminally coupled sets are {8.08, 4.97} and {7.01, 4.56}. Selective ^{19}F decoupling experiments at -80 °C revealed the approximate coupling constants given in Table VI where nuclei labels correspond to those in Figure 1. Low-temperature ^{19}F NMR spectra (Figure 4) are also in accord with structure **4**. AB patterns (339.35 MHz, -90 °C) are observed for the central CF_2 group of the $-(CF_2)_3-$ segment (-129.68, -130.52, J = 282 Hz) and for the two different CF_2 groups of the four-membered ring (-111.94, -113.35, J = 195 Hz, and -116.50, -118.67, J = 198 Hz, with small vicinal coupling also observed). Overlapping AB patterns (with additional

(33) Hydrogens involved in hydrogen-bonding situations exhibit downfield shifts. See, for example: Clark, D. R.; Emsley, J.; Hibbert, F. *J. Chem. Soc., Chem. Commun.* **1988**, 1252. R. K. Harris, *Nuclear Magnetic Resonance Spectroscopy*; Pitman Books Limited: London, England, 1983; p 199.

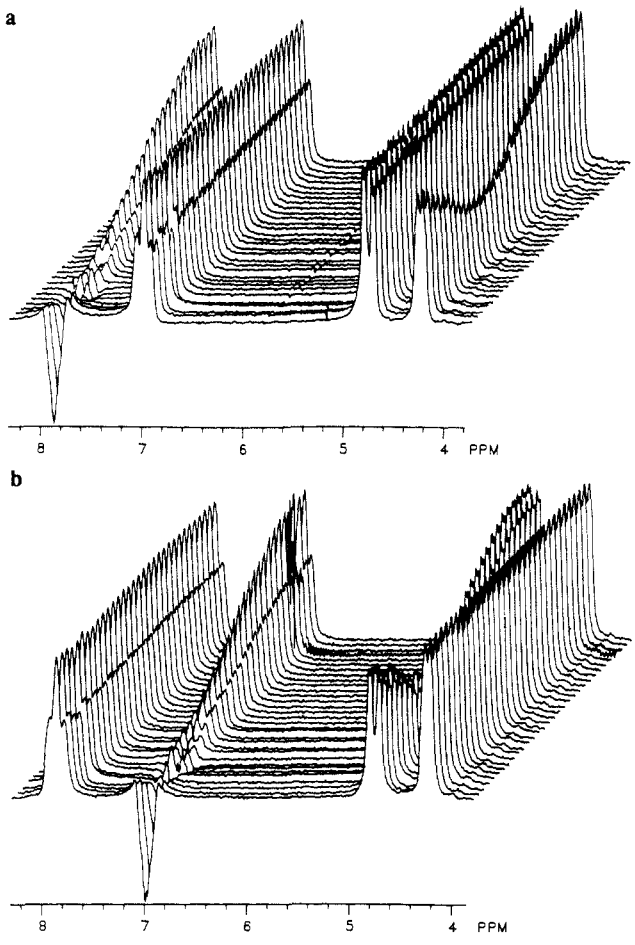

Figure 3. NMR spectra for selective inversion of protons in **4** for process 1 at −70 °C: (a) selective inversion of site **1**; (b) selective inversion of site 2. The selective inversion was obtained by means of a DANTE pulse sequence (P3 - D3) repeated 25 times, where P3 is a 4.5 μs pulse and D3 is a 200.0 μs delay. The high-power transmitter was attenuated sufficiently to produce a 90° observe pulse of 37.0 μs. Since the T_1's are approximately 0.3 s, the sum of the acquisition time and the post-acquisition delay was 1.5 s. The intervening delays following the selective inversion range from 1 ms to 3 s, with 32 times points unevenly spaced in order to map out the various exchange pathways in an optimal fashion.

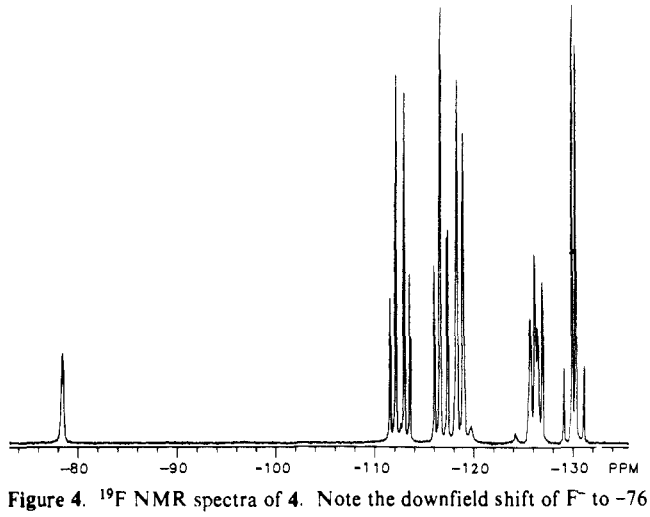

Figure 4. ^{19}F NMR spectra of **4**. Note the downfield shift of F^- to −76 ppm.

small, unresolved couplings) are also observed for the CF_2CH_2 groups: −117.12, −126.59, J = 251 Hz, and −118.79, −126.01, J = 251 Hz. The central fluoride appears as a broadened singlet at −76.6. Spectra recorded at 25 °C demonstrate that rapid site exchange takes place: ^1H NMR exhibits an averaged multiplet at 6.02, whereas ^{19}F NMR shows a somewhat broadened central F signal along with three singlets at −117.1 (8 F), −123.7 (8 F), and −131.4 (4 F).

The selective inversion/recovery method[34] was used in order to obtain mechanistic information and reliable rate constants for the dynamic processes likely to be encountered. We have focused on the lower temperature regimes (−120 to −60 °C) because the rates of exchange at these temperatures are more amenable for the inversion/recovery method and because the lower energy exchange processes are those likely to provide information about conformational changes important in forming the nest. Indeed, there are two different temperature ranges in which distinguishable types of conformational changes take place.

The lowest field ^1H signals correspond to those hydrogens bonding to the central F^- ((H9′, H18′) and (H5′, H14′) in Figure 1), and we label these pairs as sites 1 and 2. The remaining two pairs of hydrogens ((H9, H18) and (H5, H14) in Figure 1) are labeled as sites 3 and 4, and the geminally coupled nuclei correspond to sites 1,3 and 2,4. As shown in Figure 3, at −70 °C a selective transfer of magnetization occurs from site 1 to site 4. The process responsible for this exchange also interconverts sites 2 and 3. Table VII records the rate constants for transfer of magnetization[35] from site i to site j as a function of temperature. In terms of the X-ray structure labels, this result (process 1 in Table VII) demands an exchange process involving the pairs of protons H9′ and H14 (H18′ and H5) as well as H14′ and H9 (H5′ and H18). A simple enantiomerization process, consisting of a breathing motion of the 18-membered ring combined with C–C bond rotations which reverse the helical twist of the $-(CF_2)_3$ segments, readily accounts for these observations. Such a ring-torsion mode is actually found upon visualizing the lowest energy vibrational mode (18 cm^{-1}) of the complex.[31b] This process involves conformational changes coupled with H···F^- bond-breaking and regeneration of new H···F^- hydrogen bonds as a unimolecular process.

The conformational changes which occur during this enantiomerization (process 1) may be described in terms of the intraannular torsional angles (Table IV). Thus, the set of torsional angles which describes **4** (a a g− g− a a), beginning at the O1-C5 bond, is transformed to (a a g+ g+ a a). A synchronous pathway is possible, but is presumed less likely than multistep paths which minimize some of the higher energy eclipsing interactions.[29] Figure 5a shows the linear plot of ln (k) vs $1/T$ for process 1. Activation parameters are consistent with a unimolecular conformational change: $\Delta G^{\ddagger}$ (−90 °C) = 9.8 ± 0.13 kcal/mol, $\Delta H^{\ddagger}$ = 9.14 ± 1.3 kcal/mol, $\Delta S^{\ddagger}$ = −3.7 ± 6.8 eu. Control experiments using samples containing complex **4** plus 0.25 molar quantity of host **3** clearly demonstrate that low-temperature conformational changes occur without dissociation of the central fluoride, consistent with the value of $\Delta S^{\ddagger} \approx 0$. No detectable magnetization is transferred to the free host proton signal under these conditions.

^{19}F magnetization transfer experiments using the diastereotopic CF_2 signals of the four-membered rings are in qualitative agreement with the above analysis for process 1. At −70 °C, selective (partial) inversion of the "A" portion of the lower field

(34) (a) Alger, J. R.; Prestegard, J. H. *J. Magn. Reson.* **1977**, *27*, 137. (b) Led, J. J.; Gesmar, H. *J. Magn. Reson.* **1982**, *49*, 444.

(35) In all cases, the experiments reported are complete, in the sense that all the possible time dependencies that arise from single site inversion are obtained. Specifically, one data set consists of the integrated intensities as a function of time for site 1 inversion, as depicted in Figure 3a; three additional data sets are acquired at the same temperature following selective inversion at sites 2–4. The four data sets are combined and analyzed as a unit according to a model-free exchange and relaxation matrix. In this way, all possible pairwise exchange rate constants are accounted for (a 4-site exchange process has, at most, 6 independent rate constants). The rate constants thus obtained describe the three chemically reasonable processes delineated in Table VII. It would generally make more sense to report the rates of each process as a single number; if the complete data sets are analyzed by using an exchange matrix with one rate constant for each of the three processes, then appropriately weighted average values are obtained. The merit of a particular rate determination should be judged according to its associated error limit. Certain rate constants in Table VII are effectively zero and not well determined by the data.

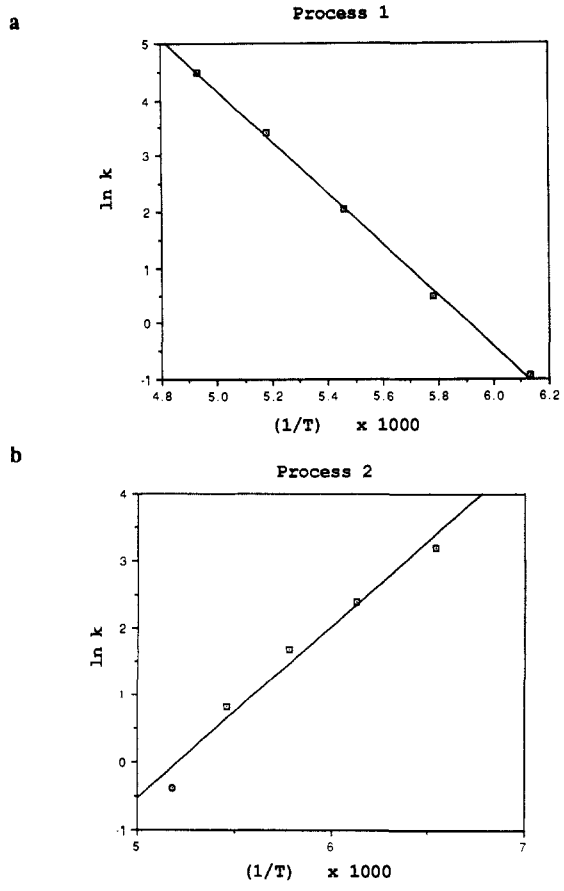

Figure 5. Arrhenius plots of the NMR inversion rate data for **4**: (a) process 1 (Note the normal behavior, increasing rates with increasing T); (b) process 2. (Note the anti-Arrhenius behavior, decreasing rates with increasing T).

AB pattern results in selective transfer to the lower-field portion of the other AB pattern. Fluorines F7 and F8 on the central carbon of the $-(CF_2)_3-$ fragment remain invariant under the operation of the above enantiomerization process. Although inversion/recovery methods were not successful for the pair (F7, F8) because of the similarity of chemical shifts and correspondingly long times required for selective inversion, the rate of exchange of these nuclei can be estimated at the coalescence temperature (−25 °C). Extrapolation of the proton data to −25 °C for process 1 gives a rate for proton exchange (sites 1 and 4) that is four times greater than the rate of exchange of F7, F8.[36] It is important to note that the temperature regimes for process 1 and that involving interchange of F7 and F8 are different and we do not have overlapping rate data. We believe that the process leading to exchange of F7 and F8 corresponds to another conformational process with an unknown rate/temperature profile. Other processes which render all hydrogens equivalent are accessible at higher temperatures, and these may include, for example, fluoride dissociation or multiple cyclobutene ring flips which break the syn arrangement of the rings.

As shown in Figure 6, a second exchange process (2) can be observed. Between −90 °C and −100 °C, a crossover in the identity of the kinetically favored proton exchange partners occurs. Below −100 °C, the largest rate constant is associated with exchange process 2 between sites 1 and 3, and 2 and 4, respectively (Table VII). Surprisingly, the rate constant for this exchange *increases* as the temperature *decreases* (Figure 5b) in clear contrast to the result observed for process 1 (Figure 5a).[37] Anti-Arrhenius behavior is infrequently encountered,[38,39] and identified examples in conformational analysis problems are very rare.[40,41] Several potentially complicating factors may play a role in this unusual behavior such as competing processes,[42] differential solvation (which might effectively change the molecularity of the process with respect to solvent), orientation effects involving the cation or multistep phenomena.

The exchange rates differ by 10% or less upon changing substrate concentration by a factor of 10. Profiles of magnetization transfer rates are very similar in three solvents, ethyl ether-d_{10},

(36) The approximate rate constant for site exchange of F7/F8 was obtained by using the equation: $k = \pi[0.5[(\delta\nu)^2 + 6J_{AB}^2]]^{1/2}$; Sandstrom, J. *Dynamic NMR Spectroscopy*; Academic Press: New York, 1982; p 84.

(37) An obvious alternative is that we are in fact observing a negative NOE which cannot be distinguished from magnetization transfer arising from chemical exchange. The role of a negative NOE can be largely ruled out on the basis of the following considerations. First, taking into account the size of the molecule, the solvent viscosity and the field strength, it is easy to show that $\omega_0\tau_c \cong 1$, and on this basis any NOE that might be observed should be very near zero. In fact, at the lowest accessible temperatures, selective inversion of a given site leads to intensity decreases in the range of 40% for the geminal partner and 20% for the remaining sites. These net results would be anomalously large even in the extreme narrowing limit, where NOE's between geminal partners are typically 15% and between more distant protons around 3–5%. On the other hand, exchange effects of the stated magnitude are very common. Second, the exchange rates reported at −120 °C are comparable in magnitude to H–F coupling constants and should, therefore, bring about conventional lineshape changes over and above any line broadening due to increased solvent viscosity. The line widths at the four methylenic proton sites do increase upon going from −110 to −120 °C, and partial line-shape analysis indicates that the T_2 derived from the line width of the TAS methyl resonance is insufficient to account for the observed broadening. It is, therefore, concluded that exchange rates of a magnitude similar to those reported in Table VII account for the observed results. Complete line-shape analysis requires a nonmutual exchange mechanism for a minimum of 6 spins (i.e., the four exchanging protons and two additional fluorines). Unfortunately, the magnitude of this problem falls outside the bounds of commonly available programs for line-shape analysis. In order to pursue this problem, we have modified the program DNMR4, and the complete line-shape analysis is in progress. It is also noted that rotating frame NOE experiments could distinguish between NOE and exchange since, in the rotating frame, the NOE is monotonically positive.

(38) Recombination processes sometimes exhibit this behavior. For recent recombination examples and discussion, see: (a) Wang, J.; Doubleday, C., Jr.; Turro, N. J. J. *J. Am. Chem. Soc.* **1989**, *111*, 3962. (b) Olson, J. B.; Koch, T. H. *J. Am. Chem. Soc.* **1986**, *108*, 756. (c) Griller, D.; Perkins, M. J. *J. Am. Chem. Soc.* **1980**, *102*, 1354. (d) Turro, N. J.; Lehr, G. F.; Butcher, J. A., Jr.; Moss, R. A.; Guo, W. *J. Am. Chem. Soc.* **1982**, *104*, 1754. (e) Houk, K. N.; Rondan, N. G. *J. Am. Chem. Soc.* **1984**, *106*, 4293. (f) Doubleday, C., Jr.; Camp, R. N.; King, H. F.; McIver, J. W., Jr.; Mullally, D. *J. Am. Chem. Soc.* **1984**, *106*, 447. Certain catalytic processes (see Paal, Z. J. *Catalysis* **1985**, *91*, 181) and *n*-butyl aminolysis of *p*-nitrophenyl trifluoroacetate (Singh, T. D.; Taft, R. W. *J. Am. Chem. Soc.* **1975**, *97*, 3867) also exhibit anti-Arrhenius behavior. A negative "activation energy" has been found for the living, anionic polymerization of styrene. See Szwarc, M. *Acc. Chem. Res.* **1969**, *2*, 87 for discussion of this classic case.

(39) (a) Glasstone, S.; Laidler, K. J.; Eyring, H. *The Theory of Rate Processes*; McGraw-Hill: New York, 1941; pp 272–281. (b) Gershinowitz, H.; Eyring, H. *J. Am. Chem. Soc.* **1935**, *57*, 985. (c) Laidler, K. J. *Chemical Kinetics*, McGraw-Hill: New York, 1965; pp 137–143. In fact, the reaction $2NO + O_2 \rightarrow 2NO_2$ has this type of behavior with $E_a \approx 0$ kcal/mol. For the $2NO + Cl_2 \rightarrow 2NOCl$ reaction, $E_a = 4.8$ kcal/mol and a normal Arrhenius behavior is observed. (d) Benson, S. W. *The Foundations of Chemical Kinetics*; McGraw-Hill: New York, 1960; pp 305–316. (e) Johnston, H. W. *Gas Phase Reaction Rate Theory*; Ronald Press: New York, 1966; Chapter 14, pp 253–262.

(40) Large activation entropies for conformational process are usually considered suspect (see, for example, ref 30). There are examples of bond rotation processes with large negative ΔS^*, but these effects are ascribed to an increased order in the solvent cage surrounding molecules in a (polarized) transition state (see: Belsky, I.; Dodiuk, H.; Shvo, Y. *J. Org. Chem.* **1977**, *42*, 2734. Dreier, C. D.; Henriksen, L.; Karlsson, S.; Sandstrom, J. *Acta Chem. Scand. B* **1978**, *32*, 281).

(41) Some conformational equilibria are entropically determined. Examples include certain cavitands whose conformers are believed to differ with respect to solvation (see: Moran, J. R.; Karbach, S.; Cram, D. J. *J. Am. Chem. Soc.* **1982**, *104*, 5826) and certain small oligopeptides whose conformations are controlled by entropy contributions to the free energy (see: Laatikainen, R.; Tuppuraihen, K. *Tetrahedron Lett.* **1989**, 5021.

(42) A further difficulty with the analysis of the data is the presence of a third process (3) in which sites 1 and 2 exchange as do sites 3 and 4 (Table VII). Whereas processes 1 and 2 interconvert the protons that bind the F^- with the protons that do not bind the F^-, process 3 interconverts the distinguishable protons that bind the F^-. Process 3 has a smaller rate constant than that for process 2 between −120 °C and −90 °C but the differences are smaller at higher temperatures. In the region between −120 °C and −90 °C, the dependence of the rate constant on temperature for process 3 is the same as for process 2.

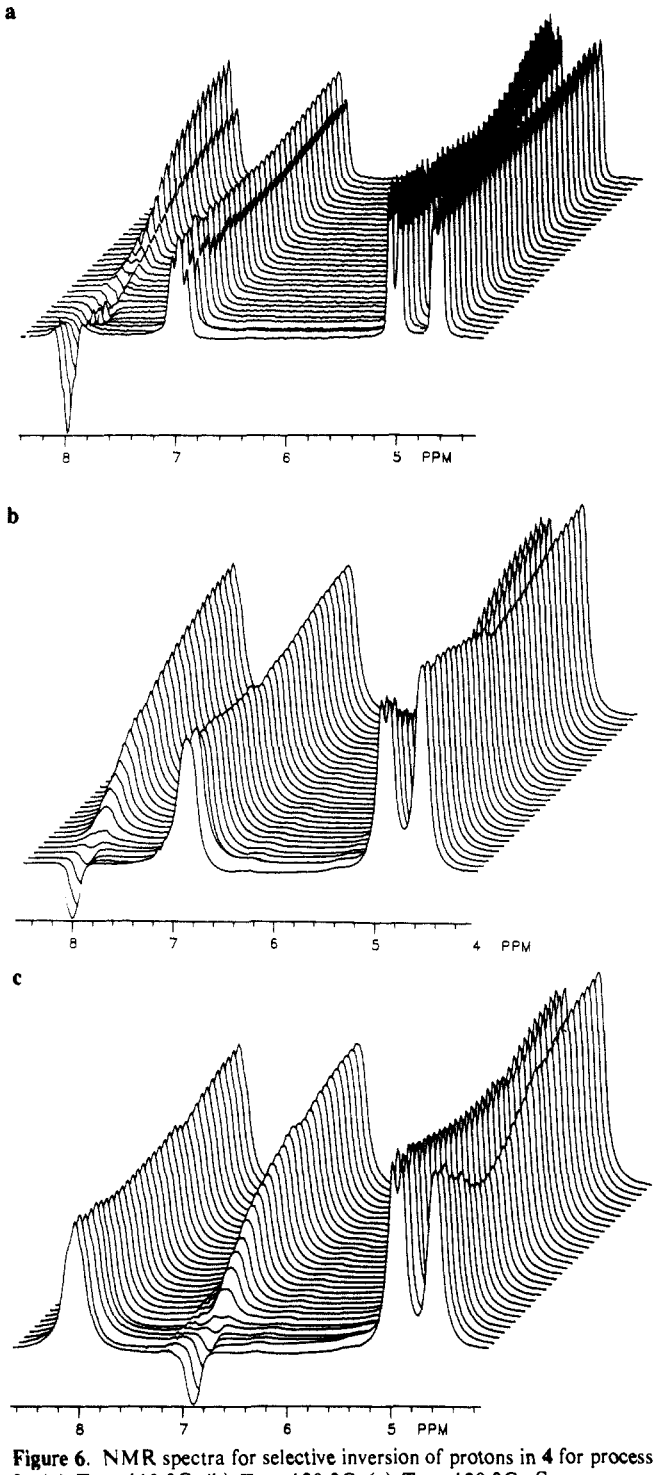

Figure 6. NMR spectra for selective inversion of protons in **4** for process 2: (a) $T = -110$ °C; (b) $T = -120$ °C; (c) $T = -120$ °C. Spectra were acquired as outlined in the caption to Figure 3.

THF-d_8/ethyl ether-d_{10}, and 1-chlorobutane-d_9. Selected temperatures were examined by using different substrate concentrations, (Table VII). Although it may be argued that chlorobutane and ether/THF do not differ much in polarity,[43] it seems unlikely that all three systems exhibit equivalent differential solvation effects as the transition state for the anti-Arrhenius process is reached. The rates of H exchange are essentially identical for complexes **4** and **5**. Thus, special cation orientation effects, which might be important in an ion-pairing phenomenon, do not appear to be of consequence.

Process 1 interconverts a proton binding the F^- with a proton on a different carbon that does not bind the F^-. Our model for this interconversion involves a series of torsions about the backbone. A geometric model of process 2 which accounts for the observed identities of exchanging nuclei (sites 1 and 3 and sites 2 and 4) for the most preferred pathway and which also leads to the same rate/temperature profile for process 3 is now described. This model consists of highly restricted sets of rotations which must be carried out in a cooperative fashion. Thus one might expect the $T\Delta S^*$ term to dominate the enthalpic contributions. Complex **4** can be converted to conformer **11** which contains only a center of symmetry by performing two operations: (1) reversing the helicity of one $-(CF_2)_3-$ fragment and (2) reorienting one cyclobutene ring such that the cyclobutene rings lie on opposite sides of the mean plane defined by the four oxygen atoms. The resulting conformation of the tricyclic system is then similar to that of the free macrocycle, except that the requisite hydrogens are pointing toward the middle of the large ring, in order to retain binding to the central fluoride ion which lies at the center of symmetry. The overall result is another enantiomerization mode, but one which proceeds though a transition state/intermediate with inversion symmetry. Conversion of complex **4** to **11** requires the site exchange of all geminal nuclei.

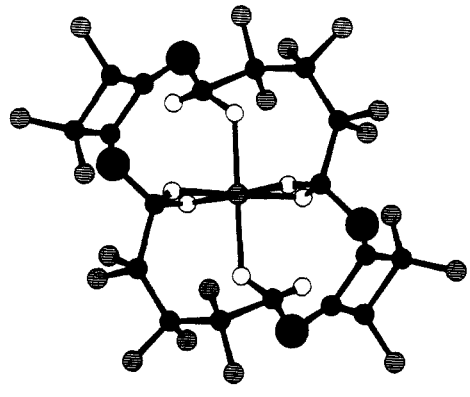

11

The ^{19}F NMR spectra are qualitatively in accord with this expectation. In contrast to the magnetization transfer results for the cyclobutenyl CF_2 AB patterns at −70 °C (e.g., $F_2 \rightleftarrows F_4$ and $F_1 \rightleftarrows F_3$, Figure 1), magnetization at −120 °C is transferred selectively between geminally related nuclei (e.g., $F_2 \rightleftarrows F_1$ and $F_3 \rightleftarrows F_4$, Figure 1). Structure **11** offers a potentially different set of coordination sites for the central fluoride; two short-range, strong interactions with, for example, H's 14′ and 5 (in "axial" locations), and weaker interaction with four other H's (9, 9′, 18, 18′) (located at "equatorial" positions in a pseudooctahedral arrangement[24]). Of course, the symmetry requirements of the exchange could be accounted for with an intermediate structure consisting of the central fluoride located at the center of inversion in macrocycle **3**. Such a structure is obviously energetically acceptable for the uncomplexed macrocycle, but seems to offer inferior binding sites for the central fluoride.[44] Inspection of molecular models suggests that, for conformer **11**, only minor torsions would then be required to exchange those protons involved in process 3.

The rate constants for process 2 (and process 3) may not correspond to a simple, fundamental reaction. For these processes, it is not difficult to envision that the cation (and possibly solvent molecules) must also reorganize as the complex undergoes its torsions because of the interaction of the captive F^- with the cation. Thus, the fundamental process may actually be of quite high molecularity as the cation and some solvent molecules must reorient. This could then lead to the unusual dependence of the rate constant on temperature. Using this rationalization, the

(43) Solvent polarity indices, E[1] (30), for ether, THF, 1-chloropropane (taken as a model for 1-chlorobutane) are 34.5, 37.4, and 37.4, respectively. See: Reichardt, C, *Solvents and Solvent Effects in Organic Chemistry*, 2nd ed.; VCH Publishers: Deerfield Beach, FL, 1988; Chapter 7.

(44) The distance between C9 and C9′ in macrocycle **3** is 6.98 Å, whereas the corresponding distances in **4** (X-ray) are 5.20 Å and 5.44 Å.

Table VII.[a,b] Rate Constants (sec^{-1}) from ^1H Selective Inversion/Recovery Experiments

temp, °C	process 1		process 2		process 3	
	$k(1 \rightarrow 4)$	$k(2 \rightarrow 3)$	$k(1 \rightarrow 3)$	$k(2 \rightarrow 4)$	$k(1 \rightarrow 2)$	$k(3 \rightarrow 4)$
			TAS; THF/Et_2O (3/1); 5.9×10^{-2} M			
-120	0.95 ± 0.70	0.47 ± 0.68	24.42 ± 0.83	24.98 ± 0.82	8.71 ± 0.85	1.16 ± 0.57
-110	0.39 ± 0.21	0.41 ± 0.21	11.23 ± 0.23	10.75 ± 0.23	4.48 ± 0.26	0.95 ± 0.17
-100	1.72 ± 0.12	1.52 ± 0.12	5.34 ± 0.12	5.31 ± 0.12	2.61 ± 0.15	0.80 ± 0.09
-90	7.14 ± 0.22	8.20 ± 0.24	2.18 ± 0.20	2.32 ± 0.21	1.18 ± 0.24	0.92 ± 0.18
-80	32.60 ± 0.87	27.97 ± 0.70	0.50 ± 0.59	0.88 ± 0.63	1.14 ± 0.62	1.32 ± 0.59
-70	95.64 ± 4.79	83.25 ± 4.36	0.85 ± 3.34	0.10 ± 3.36	0.10 ± 3.31	2.90 ± 3.39
			TAS; THF/Et_2O (1:1); 5.9×10^{-2} M or 1.5×10^{-2} M			
-110	0.23 ± 0.17	0.25 ± 0.16	4.40 ± 0.17	4.28 ± 0.18	1.90 ± 0.21	-
-100	1.55 ± 0.10	1.72 ± 0.10	1.96 ± 0.10	1.78 ± 0.10	1.26 ± 0.13	0.48 ± 0.08
-90	8.36 ± 0.18	7.77 ± 0.17	0.93 ± 0.16	0.48 ± 0.15	0.94 ± 0.18	0.76 ± 0.14
			TAS; Et_2O; 1.4×10^{-2} M			
-110	0.02 ± 0.06	0.20 ± 0.06	2.30 ± 0.06	2.23 ± 0.06	1.23 ± 0.07	0.08 ± 0.04
-100	-	-	0.83 ± 0.06	0.60 ± 0.06	0.38 ± 0.08	-
-90	1.01 ± 0.06	1.07 ± 0.07	-	-	-	-
-80	5.69 ± 0.20	5.50 ± 0.20	-	-	-	-
-70	22.62 ± 0.61	22.02 ± 0.60	-	-	-	-
			TPS; Et_2O; 2.6×10^{-2} M			
-110	0.14 ± 0.08	0.15 ± 0.08	3.01 ± 0.08	2.71 ± 0.08	1.44 ± 0.10	0.20 ± 0.01
-70	73.53 ± 2.69	70.76 ± 2.54	0.20 ± 1.98	0.02 ± 1.98	0.07 ± 2.03	0.36 ± 1.92
			TPS; chlorobutane; 2.1×10^{-2} M			
-110	1.10 ± 0.32	0.46 ± 0.33	11.17 ± 0.37	10.63 ± 0.36	2.94 ± 0.41	0.59 ± 0.26
-70	69.12 ± 4.75	78.39 ± 4.55	-	5.54 ± 3.59	4.42 ± 2.82	2.64 ± 4.20

[a] The heading for each group of rate constants indicates the cation, solvent, and complex concentration employed. [b] Dashed line entries indicate values not determined.

different rate processes involve different kinds of cation and solvent interactions because in process 1 we observe a "normal" Arrhenius dependence whereas for processes 2 and 3, non-Arrhenius behavior is observed.

Termolecular reactions often show unusual dependencies of the rate constant with temperature. For example, the usual rate expression for a bimolecular reaction has a factor of kT/h before the preexponential factor with the remaining part of the preexponential factor having a temperature dependence of $\sim T^{-1}$ giving a preexponential factor that is essentially independent of T. However, the treatment for a termolecular reaction gives a very different expression for the preexponential factor. The expression for three diatomic molecules in a nonlinear complex leads to a temperature dependence for k of $T^{-7/2}e^{-E_a/RT}$. Thus for values of E_a that are near zero (or small), the rate is expected to decrease as the temperature increases. Such behavior has been seen in the nitric oxide/oxygen reaction or in atom recombination reactions.[39]

With the aim of achieving further understanding of the three processes, the deuterated complex **4**-d_8 was synthesized.[45] NMR experiments were carried out to determine deuterium isotope effects in the conformational processes described above. A "mixing" experiment using equimolar quantities of **4**-d_8 and **3** in THF-d_8 (measuring the ratio **3**/**4** at -80° and -60 °C by ^1H NMR) showed no thermodynamic preference for deuterium or hydrogen bonds to the central fluoride. The measured equilibrium constant for reaction 7 (0.93) is probably within experimental error of 1.0. Rates of fluorine nuclei exchange corresponding to the

$$\mathbf{4}\text{-}d_8 + \mathbf{3} \rightleftharpoons \mathbf{4} + \mathbf{3}\text{-}d_8 \qquad (7)$$

conformational processes described above (-90 to -20 °C) were similar for **4** and **4**-d_8.[47]

We attempted to assess the fluoride binding energy of complex **4** (i.e., the fluoride affinity of macrocycle **3** as indicated in eq 8), by examining the kinetics of the degenerate exchange process of eq 9. A solution of complex **4** and macrocycle **3** was prepared

$$\text{complex } \mathbf{4} \rightarrow \text{macrocycle } \mathbf{3} + F^-/TAS^+ \qquad (8)$$

$$\text{complex } \mathbf{4} + \text{macrocycle } \mathbf{3} \rightarrow \text{macrocycle } \mathbf{3}' + \text{complex } \mathbf{4}' \qquad (9)$$

in 1/1 THF/ether such that [**4**] = 7.9×10^{-2} M and [**3**] = 6.1×10^{-3} M. ^1H NMR spectra were recorded at -80 to +20 °C, and lineshape analysis was carried out by using the procedures described in the Experimental Section. Activation parameters for this process are $\Delta G^{\ddagger}$ (-10 °C) = 12.2 kcal/mol; $\Delta H^{\ddagger}$ = 16.8 kcal/mol; $\Delta S^{\ddagger}$ = 17.8 eu.[48] Considering the simplifications made in the band-shape-fitting procedure and the relative simplicity of the two-line spectrum, systematic errors may be present in these values for $\Delta H^{\ddagger}$ and $\Delta S^{\ddagger}$. It should be noted that a moderately large positive value for $\Delta S^{\ddagger}$ would be anticipated for a dissociative process; not only are additional particles produced, but also *increased* conformational flexibility should be realized at the transition state leading to free macrocycle **3**. The role of sovent and its effect upon derived activation parameters remains unknown. More importantly, we observed that the line shape depends on the concentrations of **3** and **4**, indicative of some bimolecular exchange. Thus, the activation energy for the degenerate exchange process provides only an approximate lower limit for the fluoride binding energy of complex **4** in solution. The value of 16.8 kcal/mol is about 12 kcal/mol less than our estimated gas-phase value for the fluoride affinity of **3**. Considering the difference

(45) Lithium aluminum deuteride reduction of commercially available perfluoroglutaryl chloride afforded 2,2,3,3,4,4-hexafluoro-1,5-pentanediol-d_4 which was converted to the macrocycle **3**-d_8 by using the reaction sequence described for **3**. Direct comparison of Raman spectra for the free macrocycle and the (TAS) fluoride complex was now possible without interfering C-H bands. The spectrum of the free macrocycle **3**-d_8 (supplementary material) exhibits a complex series of C-D stretching bands from 2288 to 2080 cm^{-1}. The spectrum of **4**-d_8 exhibits a much broader absorption in the C-D stretching region from 2264 to 2020 cm^{-1}. The C=C stretch for the complex is shifted to lower energy by 12 cm^{-1} (1753 to 1741 cm^{-1}). Although these spectral changes are indicative of hydrogen-bond formation, they provide no information about bond energies or formation constants.[46]

(46) (a) Green, R. D. *Hydrogen Bonding By C-H Groups*; John Wiley and Sons: New York, 1974. (b) Li, C.; Sammes, M. P. *J. Chem. Soc., Perkin Trans. 1* **1983**, 1303. (c) Slasinski, F. M.; Tustin, J. M.; Sweeney, F. J.; Armstrong, A. M.; Ahmed, Q. A.; Lorand, J. P. *J. Org. Chem.* **1976**, *41*, 2693. (d) Relative strengths of deuterium vs hydrogen bonds appear to depend upon the system investigated. See: Joesten, M. D.; Schaad, L. J. *Hydrogen Bonding*; Marcel Dekker, Inc.: New York, 1974, p 182.

(47) Even though small isotope shifts were evident at lower temperatures (ca. -80 °C), ^{19}F line shapes were nearly the same for **4** and **4**-d_8 at intermediate and higher temperatures.

(48) Rate constants in per second for reaction 9: 30 (-30 °C), 105 (-20 °C), 475 (-10 °C), 1500 (0 °C), 4500 (10 °C).

in phases and the semiquantitative computational values, the qualitative similarity of the results is reasonable.

Conclusions

Macrocyclic polyether **3** is an unusual host for the binding of a fluoride ion. The host undergoes a number of conformational changes in order to bind the fluoride by four C-H hydrogen bonds. The fluorinated groups attached to the $-CH_2-$ groups constitute the electronic driving force for binding of the fluoride and simultaneously provide stereochemical labels in the resulting complex. Several enantiomerization processes that are nondissociative feature hydrogen bond making and breaking steps coupled with multiple bond rotations. Anti-Arrhenius behavior is associated with some of these conformational processes. This suggests that solvent and/or gegenions are involved in the conformational changes and that the complete supersystem may need to be included for a complete analysis of the data. Theoretical model calculations were useful in understanding some of the modes leading to enantiomerization and in providing insight into the bonding and energetics of the complex. Extension of these results to other systems with sufficiently low energy barriers and restricted conformational spaces should provide other examples which exhibit unusual conformational dynamics with novel temperature dependencies.

Acknowledgment. We wish to acknowledge Steve Zane and Lou Lardear for technical assistance. Dr. Bruce Chase kindly provided Raman data for **3** and **4**. B. E. Smart, T. Fukunaga, J. D. Roberts, G. M. Whitesides, and N. J. Turro provided helpful discussion.

Supplementary Material Available: Tables of fractional coordinates and thermal parameters, intramolecular bond distances and angles, and intermolecular distances for **3-5** (34 pages); listing of structure factors for **3-5** (30 pages). Ordering information is given on any current masthead page.

Oriented Crystallization as a Tool for Detecting Ordered Aggregates of Water-Soluble Hydrophobic α-Amino Acids at the Air-Solution Interface

I. Weissbuch,* F. Frolow, L. Addadi,* M. Lahav,* and L. Leiserowitz*

Contribution from the Structural Chemistry Department, The Weizmann Institute of Science, Rehevot 76100, Israel. *Received January 31, 1990*

Abstract: The formation of two-dimensional ordered aggregates of water-soluble hydrophobic α-amino acids at the air-solution interface has been demonstrated through the induced epitaxial nucleation of α-glycine crystals at these interfaces. This crystallization method, albeit indirect, has been found to be very sensitive to small changes in the structure of the presumed aggregates. The hydrophobic-amino acids used were divided into two classes: The first, including valine, leucine, phenylalanine, norleucine, isoleucine, and α-aminooctanoic acid, induced fast oriented crystallization of α-glycine, at the solution surface, whereas the second class, *tert*-butylglycine, neopentylglycine, and hexafluorovaline, did not. The comparison between the packing arrangement of the α-glycine crystalline face attached at the interface and that of various hydrophobic α-amino acid crystals, complemented by surface tension measurements, brought evidence in favor of the formation of structured domains which must carry precise enantioselective information to generate the oriented crystallization process. These results may be relevant to any process involving structural self-aggregation.

Introduction

Information available today on the initial stages of aggregation of molecules either at interfaces or in the bulk solution is sparse. These processes are decisive for the formation of membranes, thin molecular films, and crystals and are therefore important in fields ranging from biochemistry to the material sciences.

It is well-known that water-soluble amphiphiles have a tendency to accumulate at the air-solution interface. Surface tension[1] and other modern experimental techniques such as nonlinear optic measurements[2] and X-ray[3] and neutron specular reflectivity[4,5] have been used to provide direct information both on the surface concentration and on the orientation of such molecules. None of these techniques is however sensitive to the distribution of the molecules within the surface layer.

The question we pose here is whether water-soluble hydrophobic α-amino acids form two-dimensional-ordered aggregates or are randomly distributed at the air-solution interface. It is our hypothesis that spontaneous organization of water soluble hydrophobic α-amino acids can occur at the air-solution interface, yielding aggregates with a layer structure similar to that found within the crystals of the same compound. We further obtained evidence from previous studies[6-8] that crystal nuclei assume structures similar to that of the mature crystals. If both these assumptions are true, the above-mentioned aggregates may serve as structured two-dimensional domains for epitaxial nucleation of the same compound or of other compounds, provided a structural match exists between the structures of the two crystals within the interface layer.

Following this line of thought we use here the induction of oriented floating glycine crystals of the α form by soluble hy-

(1) Pappenheimer, J. R.; Lepie, M. P.; Wyman, J., Jr. *J. Chem. Soc.* **1936**, *58*, 1851-1855.
(2) Hicks, J. M.; Kemnitz, K.; Eisenthal, K. B.; Heinz, T. F. *J. Phys. Chem.* **1986**, *90*, 560-562.
(3) Weissbuch, I.; Addadi, L.; Als-Nielsen, J.; Kjaer, K.; Lahav, M.; Leiserowitz, L. Unpublished results.
(4) Lee, E. M.; Thomas, R. K.; Penfold, J.; Ward, R. C. *J. Phys. Chem.* **1989**, *93*, 381-388.
(5) Bradley, J. E.; Lee, E. M.; Thomas, R. K.; Willatt, A. J.; Gregory, D. P.; Penfold, J.; Ward, R. C.; Waschkowsky, A. *Langmuir* **1988**, *4*, 821.
(6) Addadi, L.; Berkovitch-Yellin, Z.; Weissbuch, I.; van Mil, I.; Shimon, L. J. W.; Lahav, M.; Leiserowitz, L. *Angew. Chem.* **1985**, *23*, 346.
(7) Weissbuch, I.; Zbaida, D.; Addadi, L.; Lahav, M.; Leizerowitz, L. *J. Am. Chem. Soc.* **1987**, *109*, 1869.
(8) Addadi, L.; Berkovitch-Yellin, Z.; Weissbuch, I.; Lahav, M.; Leiserowitz, L. *Top. Stereochem.* **1986**, *16*, 1-85.

0002-7863/90/1512-7718$02.50/0